

ASEN 3111

Computation of Potential Flow

Computational Lab # 2

September 22, 2017

Nicholas Renninger, *

I. Introduction

Problems in engineering often involve modeling complex, co-dependent phenomena that give rise to observable processes and effects. Modeling these phenomena typically involves the development of one or more partial differential equations (PDEs) and the associated boundary conditions (BCs). While these models can be incredibly complex, as is the case for problems like generalized fluid dynamics and weather modeling, simplified PDE models can often be used to great effect to gain insight into the behavior of a more generalized system. These simplification methods can be paired with numeric solution techniques to gain faster, easier insight into PDE solutions.

In this lab, we develop the basic PDE and BCs used in classical potential fluid flow theory, as well as the use of basic numeric PDE solvers, like the PDE Toolbox in MATLAB. Potential flow theory, for our purposes, is based on the assumption that the flow is both incompressible and irrotational. In addition to these assumptions, for this lab we will assume inviscid flow conditions.³ Under these assumptions, we can define the dilation of the fluid, $\nabla \cdot \mathbf{V}$, to be 0. Defining the dilation of the fluid, which is the time rate of change of volume per unit volume, to be zero guarantees the incompressibility of the fluid. The velocity potential, Φ , is only defined when the vorticity ξ of the flow ($\xi = \nabla \times \mathbf{V}$) is zero. From the definition of the velocity potential function, Φ , we know that $\mathbf{V} = \nabla \Phi$. From these two equations we develop the following PDE, known as **Laplace's Equation**:

$$\nabla \cdot (\nabla \Phi) = \nabla^2 \Phi = 0 \quad (1)$$

This equation simply states that the Laplacian (∇^2) of the potential function is always equal to zero. The goal of potential flow theory is to calculate Φ , as this allows one to calculate the velocity of the flow at every point in space. Once the flow velocity field is known, the pressure distribution about any bodies in the flow field can be calculated, which allows for the calculation of aerodynamic forces on any bodies in the flow.

While Laplace's Equation equation is a useful conceptual concept, its solution requires the definitions of certain BCs for it to be solvable. These BCs typically come from the geometry and setup of the domain over which Φ to be determined. Shown in Figure 1, the geometry of the computational domain will determine the BCs needed to solve Eqn. 1 for Φ . Along the walls, a no-penetration BC must be imposed such that fluid does not pass through the a wall that is supposed to be solid. Similarly no-penetration BCs must be

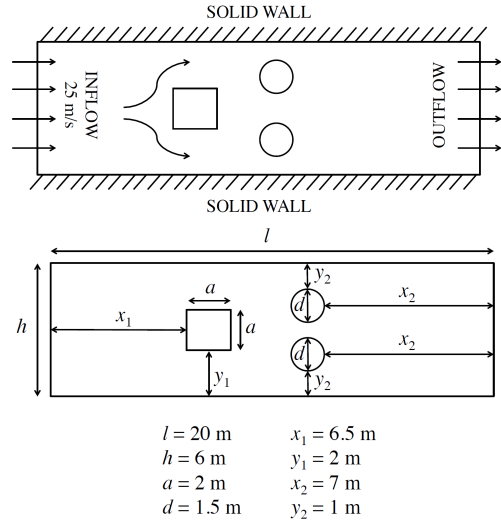


Figure 1: Fluid Flow Parameters and Test Channel Geometry. From these figures, the BCs for Eqn. 1 can be developed.

*105492876

specified for the cylinder and the square object being tested in the channel, as shown in Figure 1. Both no-penetration BCs are defined as: $\mathbf{V} \cdot \mathbf{n} = 0 = \frac{\partial \Phi}{\partial n}$. Here, \mathbf{n} represents the unit normal vector of the surfaces for which the BC is specified. Note that this BC specifies the derivative of the potential function Φ , so these BCs are called *Neumann* BCs. Next, the inflow of fluid to the channel must be specified with another BC: $\mathbf{V} \cdot \mathbf{n} = -25 \text{ [m/s]} = \frac{\partial \Phi}{\partial n}$. The normal to the inlet area, \mathbf{n} , points in the opposite direction as the inflow velocity, hence the negative sign in this BC. As this inflow velocity is time-invariant, the flow can also be assumed to be steady.³ Once again, as this BC specifies the derivative of the potential function, it is considered a *Neumann* BC. Finally, we must consider the outflow velocity from the outlet of the channel. In this case, we specify that the flow velocity must be perpendicular to the outlet area. The outflow BC is as follows, $\mathbf{V} \cdot \mathbf{s} = 0 \rightarrow \Phi = c = 0$, where \mathbf{s} is the unit tangent vector on the surface of the outlet area. We determine that as Φ is equal to some arbitrary constant c at the outlet, we can set it to $c = 0$. This BC ensures that the free-stream velocity direction in the channel, after going past the square and cylinders, returns to the free-stream velocity direction that the flow had before encountering the objects in the channel. As this BC specifies the value of Φ itself, it is not a *Neumann* BC, but rather a *Dirichlet* BC.

Now that the problem is fully specified by Eqn. 1 and its BCs given above, the PDE can be solved using the finite element method (FEM) as implemented in PDE Toolbox in MATLAB. PDE Toolbox requires the input of the PDE and its BCs, the geometry of the problem, and the mesh refinement for its FEM solver to obtain a solution. After the numeric solution is complete, the results can be plotted and analyzed. As was discussed earlier, the motivation for solving for Φ is typically to recover the flow velocity and pressure fields across the whole domain. By the definition of Φ , velocity \mathbf{V} is given by: $\mathbf{V} = \nabla \Phi$. To recover the pressure field P , we must use the fact that the flow is assumed to be incompressible, steady and inviscid for the application of Bernoulli's Equation to be valid:¹

$$P_\infty + \frac{1}{2}\rho||\mathbf{V}_\infty||^2 = P + \frac{1}{2}\rho||\mathbf{V}||^2 \quad \text{with } \mathbf{V} = u\hat{\mathbf{i}} + v\hat{\mathbf{j}} \quad (2)$$

$$\Rightarrow P = P_\infty + \frac{1}{2}\rho(||\mathbf{V}_\infty||^2 - ||\mathbf{V}||^2) = P_\infty + \frac{1}{2}\rho(||\mathbf{V}_\infty||^2 - (u^2 + v^2)) \quad (3)$$

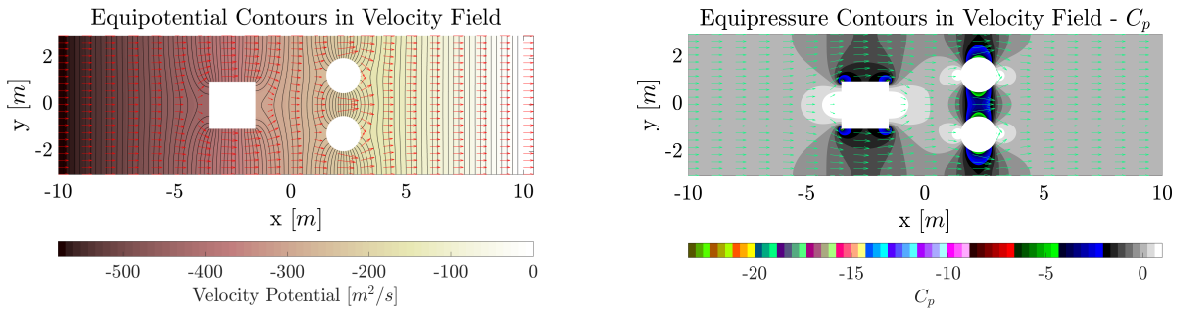
Now that an expression for pressure P has been developed with Eqn. (3), we can also develop an expression for the coefficient of pressure, C_p , that will allow us to more easily visualize and interpret the pressure field in the channel. It is defined as follows:¹

$$C_p = \frac{P - P_\infty}{q_\infty} = \frac{P_\infty + \frac{1}{2}\rho(||\mathbf{V}_\infty||^2 - ||\mathbf{V}||^2) - P_\infty}{\frac{1}{2}\rho||\mathbf{V}_\infty||^2} = 1 - \left(\frac{||\mathbf{V}||}{||\mathbf{V}_\infty||} \right)^2 = 1 - \left(\frac{\sqrt{u^2 + v^2}}{||\mathbf{V}_\infty||} \right)^2 \quad (4)$$

With Eqns. (1 - 4) and the various BCs, the full numeric solution to the potential flow problem is specified, and useful information about the flow properties is readily available. The results of this analysis are presented in the next section.

II. Results

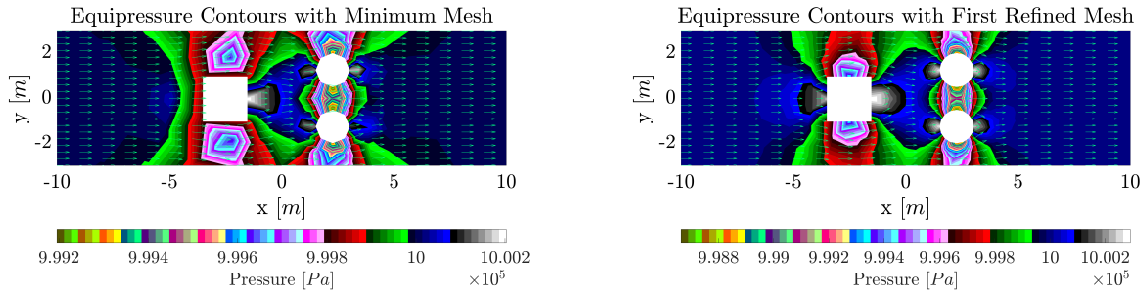
Figures (2) & (3) summarize the results of the three major analysis to be performed in this lab: to develop an analytic solution for Φ and plot the equipotential lines across the channel, to find the pressure field across the channel domain (in Figure 2b this is presented with C_p instead of P , as this makes it easier to conceptualize the pressure distribution), and to finally study the effects of mesh refinement on the stability of the numeric solution to Φ .



(a) Variation of Constant Φ Contours Across the Channel. Black lines show lines where $\Phi = \phi$, which are equipotential lines. The red arrows show $\nabla \cdot \Phi = \mathbf{V}$ and for this reason the arrows should always be normal to the equipotential lines, by the definition of the gradient operator ∇ .

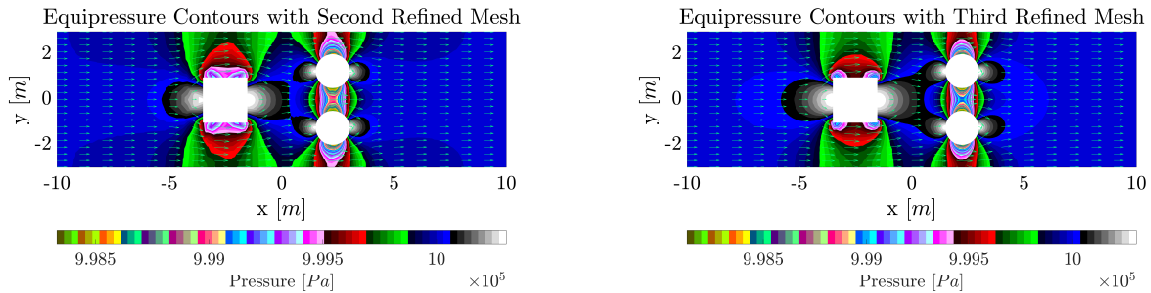
(b) Vairation of Constant C_p Contours Across the Channel. Each distinct color represents a different binned value for C_p , and the arrows once again indicate the direction of the fluid velocity vector.

Figure 2: Constant Flow Potential and Pressure Plots



(a) Pressure distribution with minimum mesh density. Note the highly irregular and non-smooth equipressure regions.

(b) Pressure distribution with 1st refinement of mesh density. Even after only moderate refinement, the solution becomes much more visually similar to the fully “converged” plot in Figure 2b



(c) Pressure distribution with 2nd refinement of mesh density.

(d) Pressure distribution with 3rd refinement of mesh density. Depending on where in the channel and along the objects one wants to determine the pressure, this refinement is relatively converged.

Figure 3: The effect of mesh refinement on the pressure distribution in the simulation

III. Conclusions

Potential flow theory offers many benefits, namely a reduction in complexity with respect to solving the full Navier-Stokes equations. In this lab, potential flow theory was developed analytically and solved numerically using the FEM in PDE Toolbox in MATLAB. A key component of the FEM, which is not treated in this report, is the generation and optimization of the computational domain's mesh. The mesh defines the domain for a series of test functions that can be used, when treated somewhat similarly to other eigenfunctions used to solve PDEs (like the fourier basis functions), to approximate the function in question over a finite area. For this reason, mesh generation is key to the successful and stable numeric solution to PDEs. In this lab, the number of elements evaluated had a visual impact on the quality of the approximation made of Φ , as shown in Figure (3). These plots demonstrate the power of the FEM method with a low quality mesh like that of Figure (3a). While the solution to the pressure field P may have been coarse, it captured the majority of the important features of the fluid flow in the channel. As mesh generation, and the solution of the PDE in question will typically require greater than linear run time, using a low quality mesh like that used in Figure (3a) for quick validation or for refinement of the solution itself might be quite useful. As the mesh refinement increases, as shown in Figures (3b - 3d), the solution converges quickly to the Pressure field shown in Figure (2b) which uses seven mesh refinements. The largest difference between Figures (2b) and (3d) is clearly demonstrated to be around the discontinuous surface of the square. The large spikes in C_p shown in Figure (4) - again using seven mesh refinements - around the square obstacle indicate the limitations of the FEM's mesh and of the incompressible potential flow theory used to model the flow. The spike occurs around the square corners because of the inability of the flow to separate or compress, and because the mesh will struggle to maintain a continuous function value over the corner domain. This problem arises frequently in discrete representations of functions, with discretization error occurring in the FEM as well as in Fourier Series. In terms of the potential flow model error, the flow must go from free stream conditions to an instantly higher velocity around the first wall in order to maintain the incompressible assumptions of Bernoulli's Equation. This unrealistic assumption also contributes to the point discontinuity clearly seen at the sharp corners of the square. As the mesh is refined, the area in the mesh over which this point discontinuity in flow velocity occurs decreases, leading to drastically increased pressure at the edges of the square (seen in the tall spikes in Figure (4) and the tiny areas of high pressure in Figure (2b)). This all means that the solutions obtained with less refined meshes are still quite useful and preserve largely the same information as the much more costly meshes produce. If one is not interested in capturing the behavior of the potential flow model and the FEM at discontinuous surfaces around the square, lower mesh refinements will result in very similar solutions to Φ for lower computational cost.

While the focus of this lab was largely on the computation of Φ , the typical quantities of interest to us as aerodynamicists are the aerodynamic forces acting on bodies in the flow. Examining Figure (2a), it can be seen that as intended by the BCs, the flow returns to the same direction that it had upon entry to the test section. Then, examining Figure (2b), C_p goes completely to 0 before and after the cylinder and square, and does not change along the walls of the channel as x increases. Also, the freestream C_p at the outlet returns to the same C_p as the inlet. This means that the flow recovers the freestream pressure after going around the objects and along the walls, which means that there is no imbalance of pressure on the objects, so there can be no pressure drag. Also, as the flow is assumed to be inviscid, there is no skin friction drag on the objects, so there is no way for there for a the flow to communicate a drag force on the objects. Once again, under incompressible, steady, inviscid flow, D'Alembert's Paradox applies² - *the total drag on the objects and walls in the channel is 0*. This result is obviously unrealistic, especially in the case of flow around a bluff body like the square. The primary reason that there is no drag on the bodies is because of the inviscid assumptions made in modeling the flow through this channel. While viscosity certainly contributes to drag through skin friction forces, it primarily causes drag (especially on bluff bodies) by causing the flow to separate. When the flow separates, the wake left behind the body causes the loss of energy in the flow, primarily in the form of pressure, due to viscous effects. This means that the distributed pressure force acting in the direction of the flow no longer is equal to the distributed pressure force along the front of the body, so the net effect is pressure drag against the direction of the flow. Therefore, as our simulation makes inviscid assumptions about the flow, there is no way for the flow to separate from the body and create drag.

Solving Laplace's Equation numerically sheds insight into the world of numerical solution of PDEs, which remains the only practical solution method for a large class of problems. However, whenever using numerical tools and simplified models, it is important to be aware of both the numeric and theoretical limitations of the models and solution methods to ensure that non-physical solutions are not taken as reality.

References

- ¹Anderson, John D. Chapter 3 Fundamentals of Aerodynamics, 5th ed., McGraw-Hill Education, 2011
- ²Anderson, John D. Chapter 5 Introduction to Flight, 8th ed., McGraw-Hill Education, 2016
- ³Evans, John. ASEN 3111 Comp. Lab 2: "Computation of Potential Flow". Lab Document. CU, 2017. PDF.

Acknowledgments

For this lab, I worked closely with Marshall Herr to develop the plotting add-ons used to produce the highly formated plots presented here in Figures (1 - 4). We devolved the formatting tools `savePDE_figs.m` and `save3dPDE_figs.m` in tandem, which is why our plots might look similar.

Appendix A: Additional Figures and Tables

3D C_p Distribution in the Channel

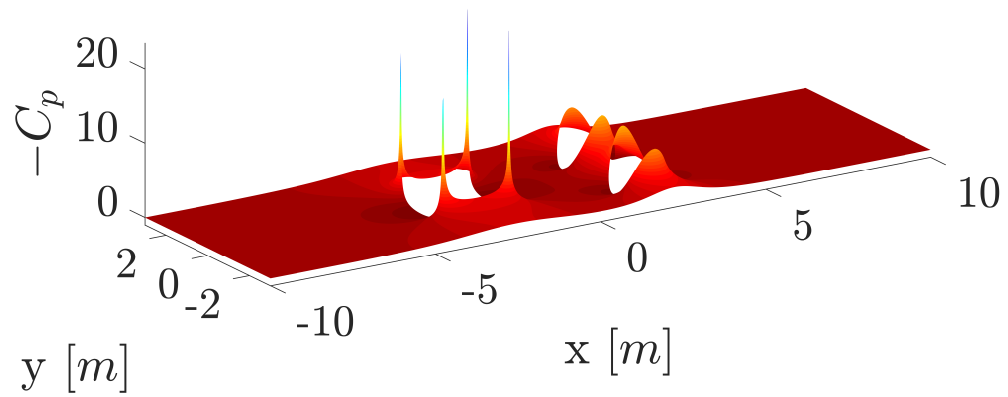


Figure 4: 3d Visualization of C_p Over the Fluid Domain.